Supporting Information

Designing Strategies for High-Redox-Potential Conjugated Carbonyl Organic Cathodes in Lithium- and Sodium-ion Batteries

Zhaoli Liu[a], Xiangyu Meng[b], Fengchao Cui*[a], and Guangshan Zhu*[a]

[a] Key Laboratory of Polyoxometalate and Reticular Material Chemistry of Ministry of Education and Faculty of Chemistry, Northeast Normal University, 5268 Renmin Street, Changchun, 130024, P. R. China.

[b] Jilin Vocational College of Industry and Technology, Jilin 132000, P. R. China.

Email: cuifc705@nenu.edu.cn & zhugs@nenu.edu.cn

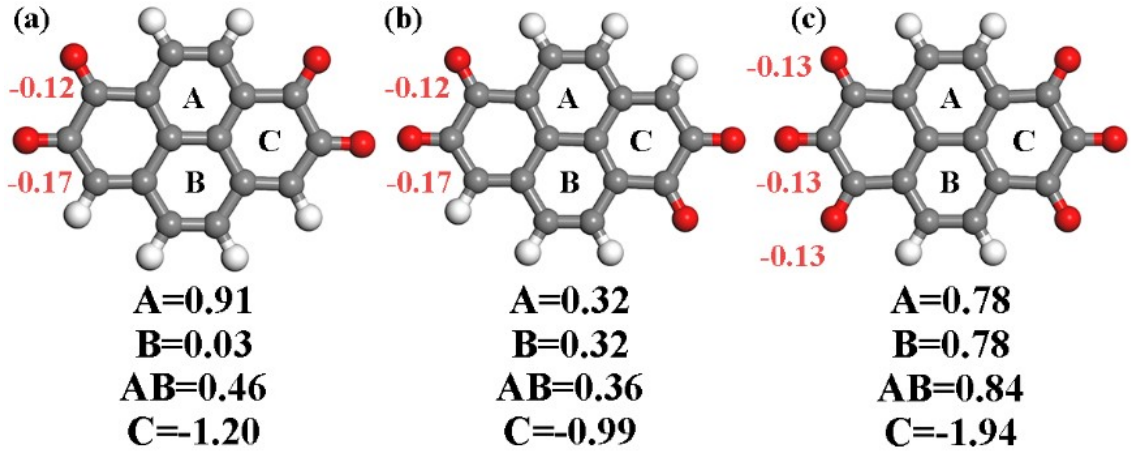

Figure S1. HOMA of various rings and BPI of various carbonyls in (a) AST, (b) BST and (c) PST, respectively. (The font color of HOMA was described in black, BPI was described in red.)

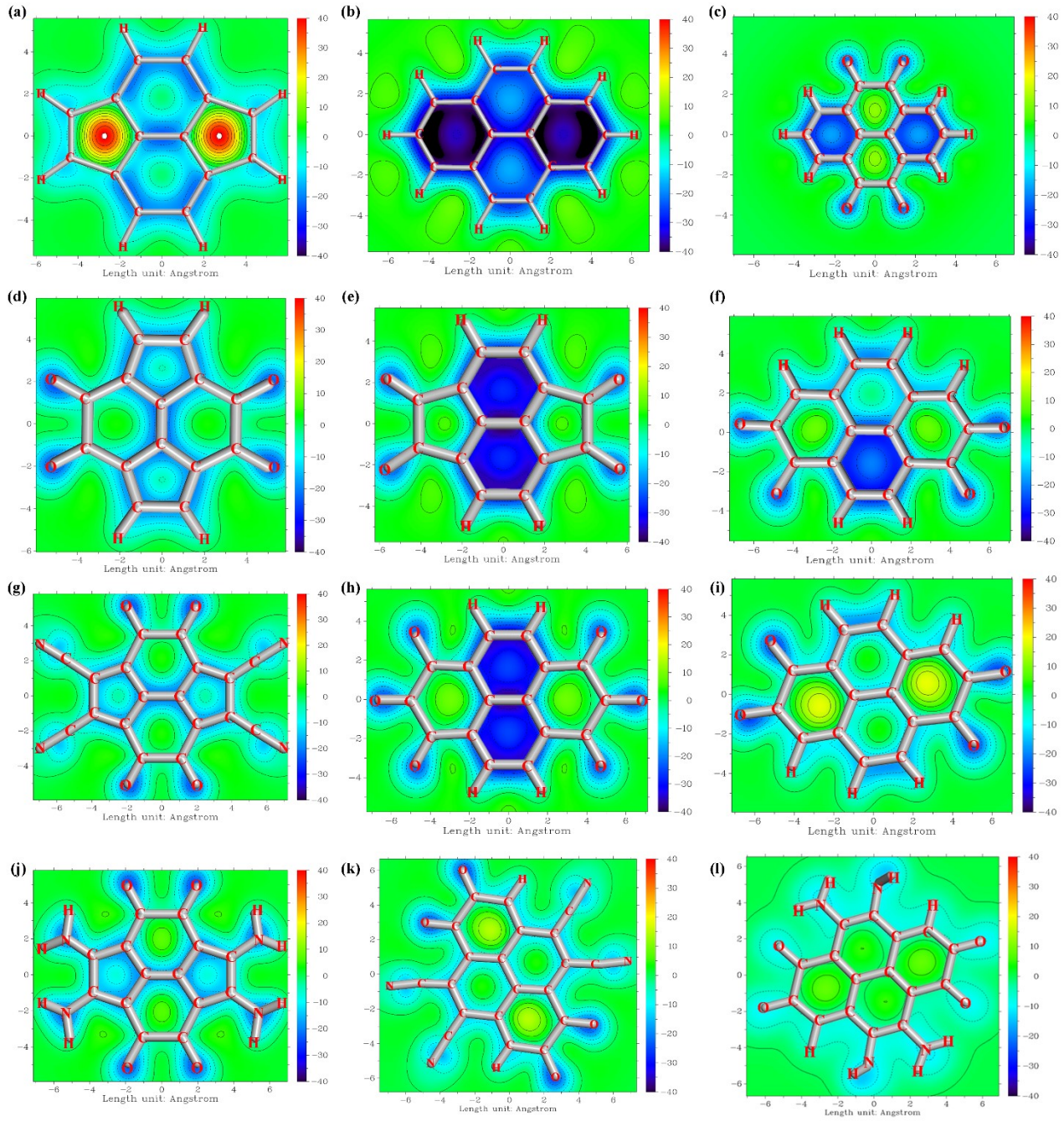

Figure S2. NICS-2D scan plane map (The ZZ component of magnetic shielding tensor above 1 Å of the plane of a ring center.) of (a) Pyracylene, (b) Pyrene, (c) PTO, (d) CAT (e) CAP, (f) AST, (g) CAT-CN, (h) PST, (i) BST, (j) CAT-NH_2, (k) BST-CN and (l) BST-NH, respectively. (The dark blue region indicates a high level of aromaticity, while the red region indicates a high level of anti-aromaticity.)

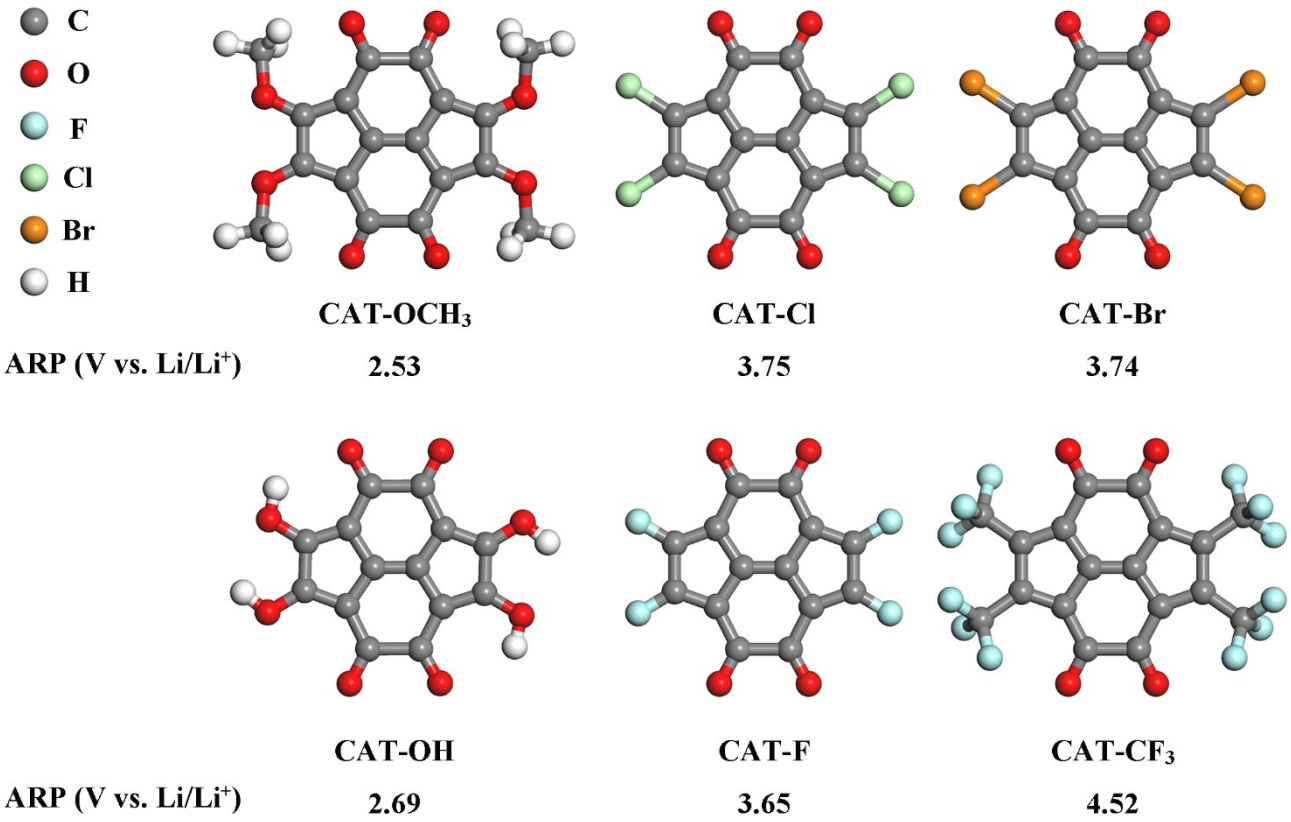

Figure S3. The structure and adiabatic redox potentials (ARP, V vs Li/Li^+) of CAT-OCH3, CAP-OH, CAT-Cl, CAT-F, CAT-Br and CAT-CF_3.

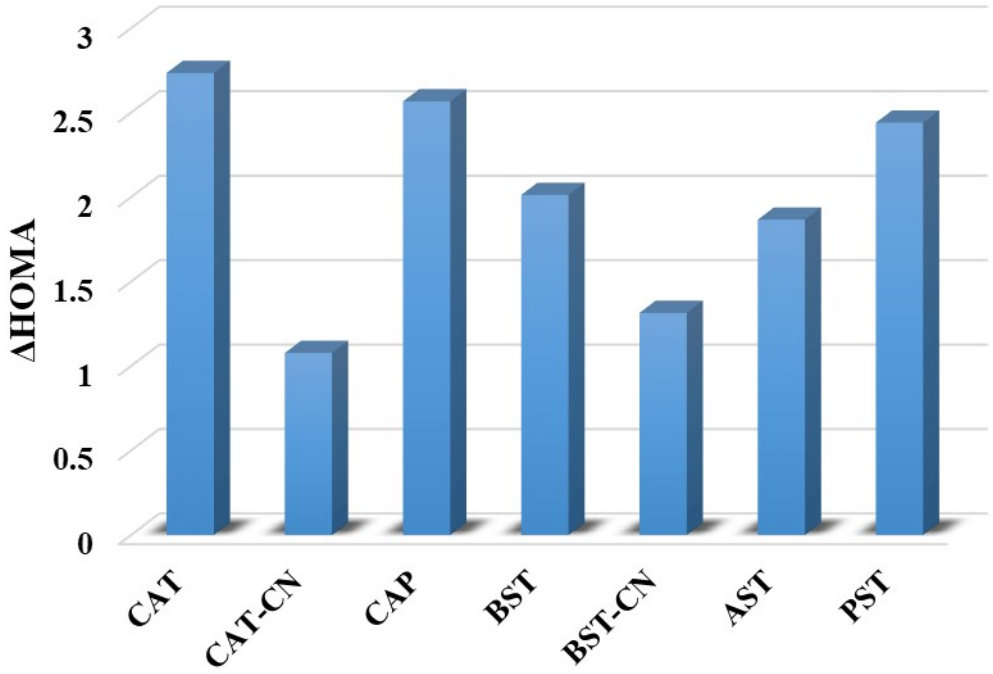

Figure S4. The difference in the Harmonic oscillator measure of aromaticity (ΔHOMA) between the fully charged states and the fully discharged states of CAT, CAT-CN, CAP, BST, BST-CN, AST and PST.

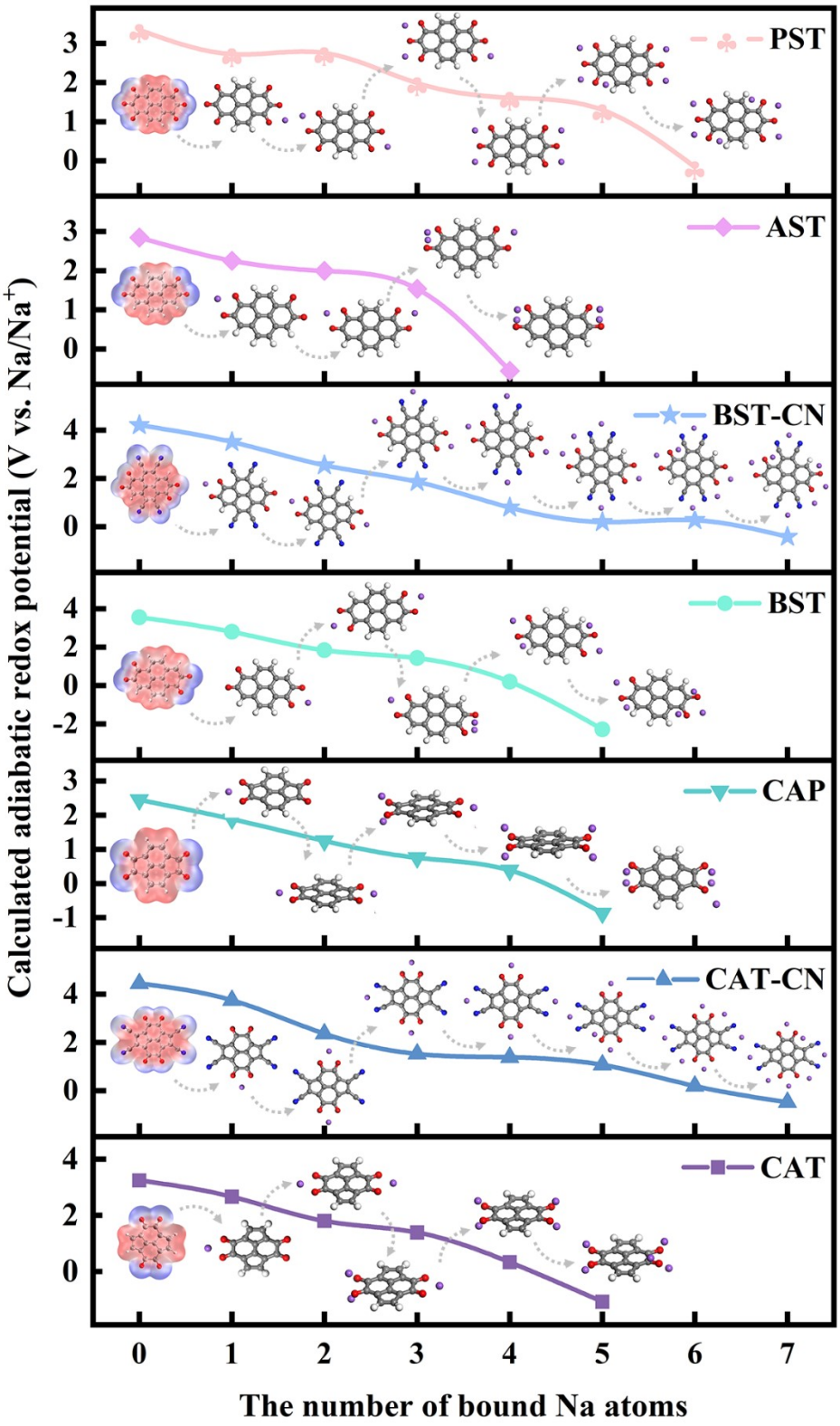

Figure S5. In the discharging process, the Na-ion storage sites and the structural evolution for seven pyrenetetrone derivatives (CAT, CAT-CN, CAP, BST, BST-CN, AST and PST) and their variety of ARP as a function of the number of bound Na atoms. (The atoms with grey, white, red, blue and purple depict carbon, hydrogen, oxygen, nitrogen and sodium, respectively.)

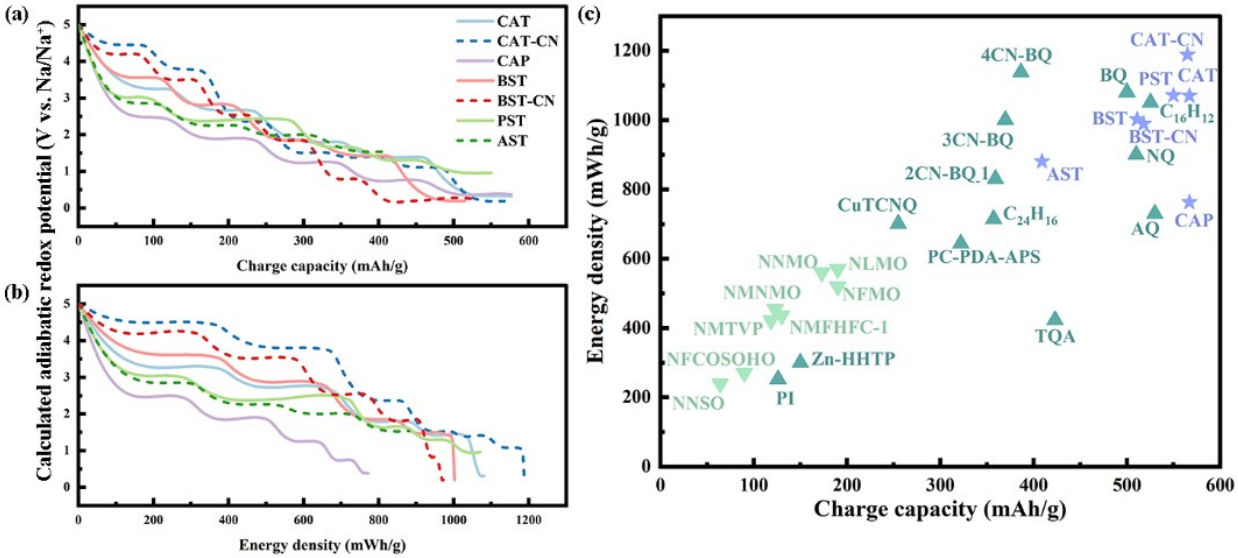

Figure S6. (a) Resultant profiles of the gravimetric charge capacities, (b) energy densities as a function of the calculated redox potential and (c) The Ragone plot shows the performance parameters of the pyrenetetrone derivatives reported by this work, the conventional inorganic compounds[1-8] and the outstanding organic compounds[9-16] referred from previous studies.

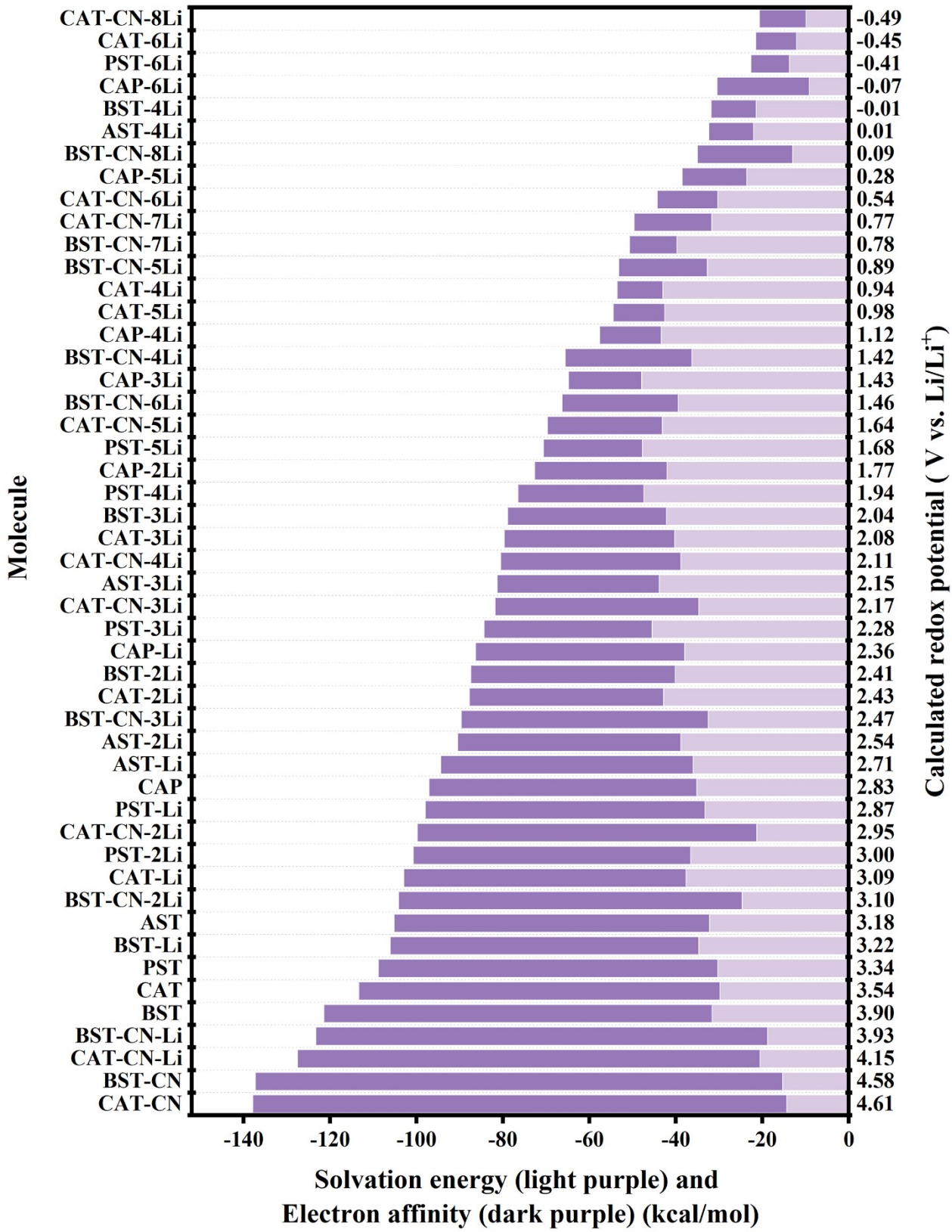

Figure S7. Contributions of solvation energy and electron affinity on redox properties. Solvation energy and electron affinity values for CAT, CAT-CN, CAP, PST, BST, BST-CN and AST with or without binding lithium atoms.

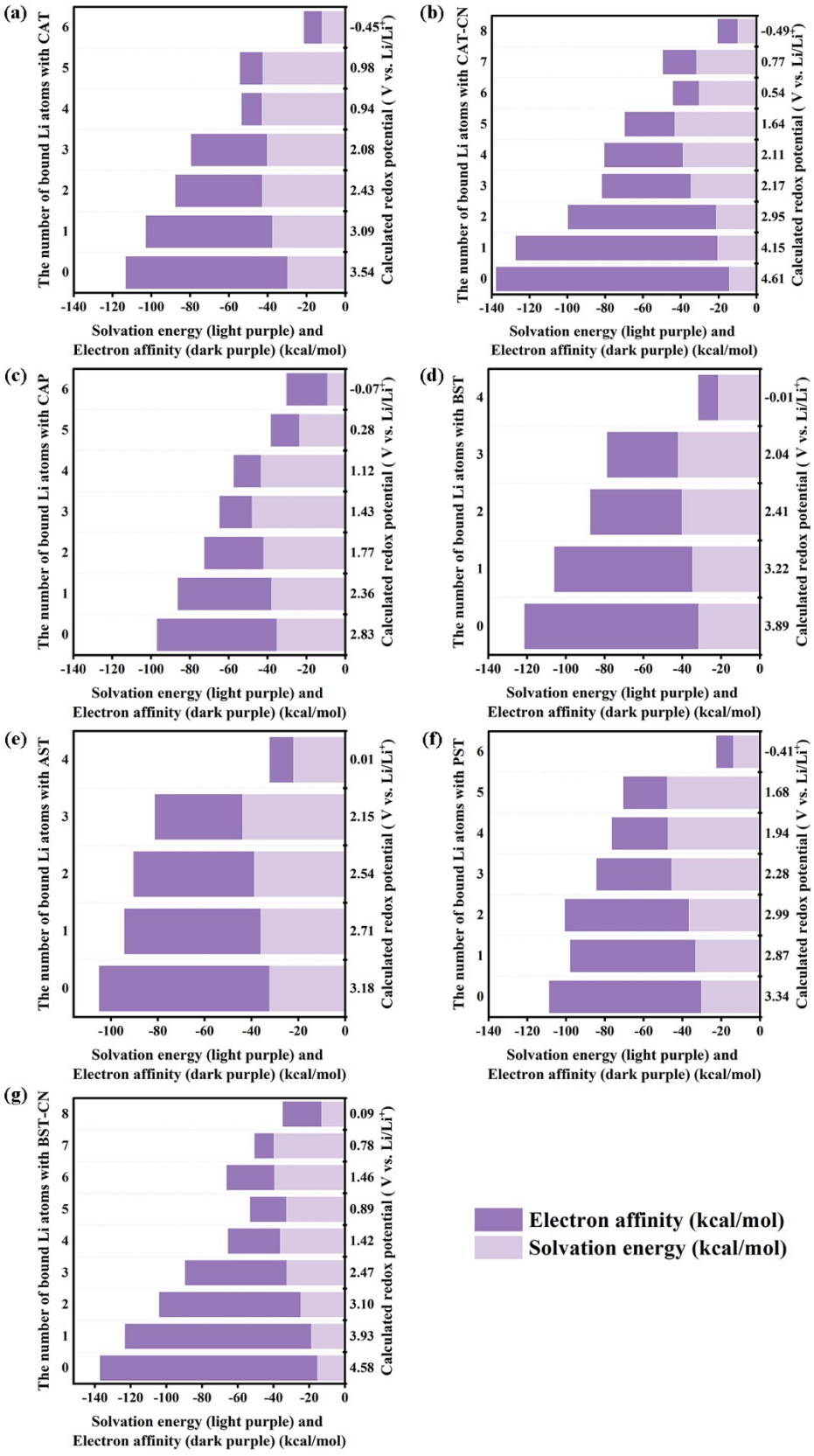

Figure S8. Contributions of solvation energy and electron affinity on redox properties. Solvation energy and electron affinity values for (a) CAT, (b) CAT-CN, (c) CAP, (d) BST, (e) AST, (f) PST and (g) BST-CN during the discharging process.

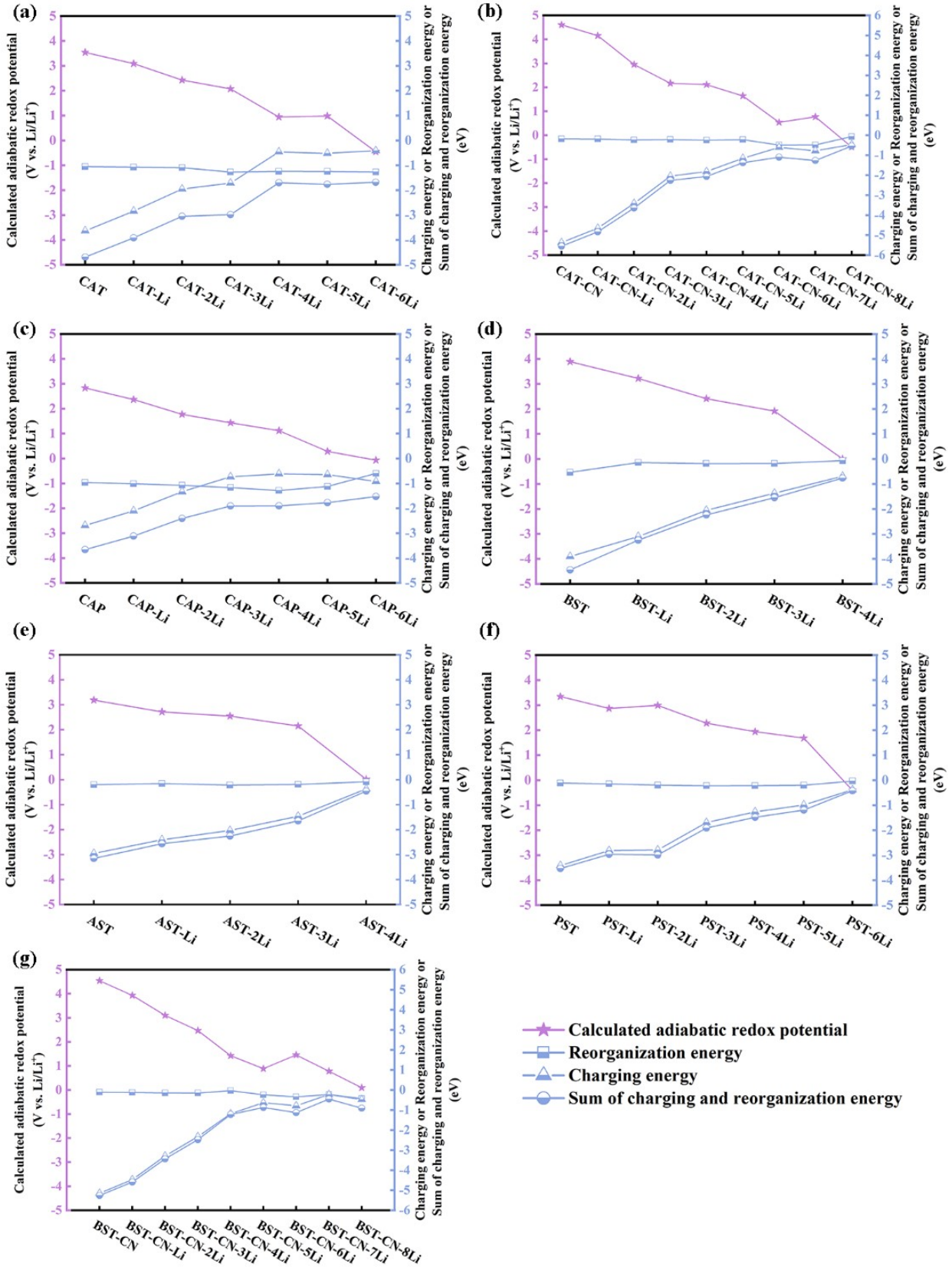

Figure S9. Contributions of charging and reorganization energies. Adiabatic redox potential, charging energy, reorganization energy, and the sum of the charging and reorganization energies for (a) CAT, (b) CAT-CN, (c) CAP, (d) BST, (e) AST, (f) PST and (g) BST-CN.

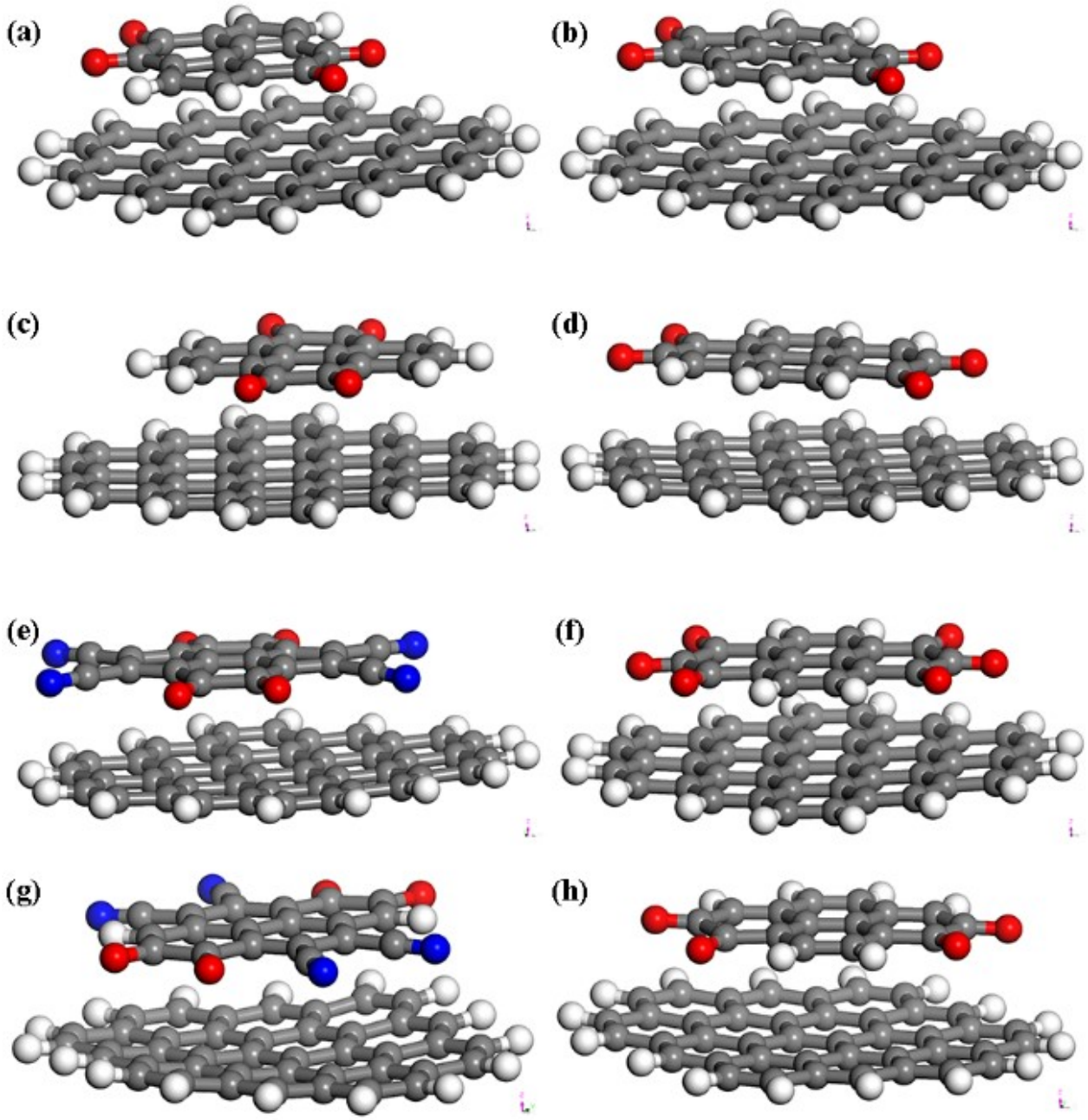

Figure S10. Cathode-graphene dimer: (a) CAT-graphene, (b) CAP-graphene, (c) PTO-graphene, (d) BST-graphene, (e) CAT-CN-graphene, (f) PST-graphene, (g) BST-CN-graphene and (h) AST-graphene.

Table S1. The comparison of the computed redox potentials for a variety of organic compounds with their experimental values. (Diff represents the difference between the computed redox potentials and their experimental values.)

Molecule	Theoretical redox potential (V vs. Li/Li^+)	Experimental redox potential (V vs. Li/Li^+)	Diff	Reference
1,4-benzoquinone	2.78	3.10	0.32	[17]
1,4-benzoquinone dimer	2.99	2.90	-0.09	[18]
1,4-naphthoquinone	2.52	2.60	0.08	[17]
9,10-anthraquinone	2.19	2.20	0.01	[17]
2-aminoanthraquinone	2.03	2.10	0.07	[17]
2,6-diaminoanthraquinone	1.84	2.00	0.16	[17]
Anthraquinone-2-carboxylic acid	2.23	2.30	0.07	[17]
1,4-bezenedicarbonitrile	1.45	1.70	0.25	[19]
Pyrenetetrone	2.62	2.59	0.03	[20]
Thiophene	-0.26	-0.10	0.16	[20]
Furan	-1.09	-1.10	-0.01	[20]
Benzopyrrole	-0.25	-0.20	0.05	[20]
Anthraquinone-1,5-disulfonic acid sodium	2.30	2.40	0.1	[21]
5,7,12,14-Pentacenetetrone	2.65	2.60	-0.05	[22]
Thianthrene-5,7,12,14-tetrone	2.82	2.90	0.08	[22]
Benzo [1,2-b:4,5-b']dithiophene-4,8-dione	2.52	2.50	-0.02	[23]
Benzofuro [5,6-b]furan-4,8-dione	2.55	2.60	0.05	[23]
Phenazine	1.79	1.90	0.11	[24]
Chloranil	3.31	3.40	0.09	[25]
2,3-Dicyano-chloranil	3.86	3.70	-0.16	[25]
Fluoranil	3.45	3.60	0.15	[25]
$(t\text{-}Bu)_3TOT$	3.06	3.10	0.04	[26]
Br_3TOT	3.41	3.60	0.19	[26]
Molecule	**Theoretical redox potential (V vs. Na/Na^+)**	**Experimental redox potential (V vs. Na/Na^+)**	**Diff**	**Reference**
9,10-anthraquinone	1.85	1.9	0.05	[27]
1,4-benzoquinone	2.44	2.8	0.36	[27]
1,4-naphthoquinone	2.18	2.3	0.12	[27]
2-aminoanthraquinone	1.69	1.8	0.11	[27]
2,6-diaminoanthraquinone	1.50	1.7	0.2	[27]
Anthraquinone-2-carboxylic acid	1.89	2.0	0.11	[27]
1,4-bezenedicarbonitrile	1.11	1.4	0.29	[19]
Thiophene	-0.60	-0.4	0.2	[28]
Furan	-1.43	-1.4	0.03	[28]
Benzopyrrole	-0.59	-0.5	0.09	[28]
Pyrenetetrone	2.11	2.2	0.09	[28]

Table S2. Atomic coordinates of AST, BST, PTO, CAP, CAT, PST, BST-CN, BST-NH_2, CAT-NH_2 and CAT-CN.

AST				BST				PTO			
	X	Y	Z		X	Y	Z		X	Y	Z
C1	0.702	0.204	0	**O1**	3.783	-1.767	0	**O1**	0	1.365	-3.574
C2	-0.702	0.204	0	**O2**	-3.783	1.767	0	**O2**	0	-1.365	-3.574
C3	1.441	1.472	0	**O3**	4.778	0.802	0	**O3**	0	1.365	3.574
C4	-1.392	-1.025	0	**O4**	-4.778	-0.802	0.001	**O4**	0	-1.365	3.574
C5	1.392	-1.025	0	**C5**	0.717	0.098	0	**C5**	0	0.736	0
C6	-1.441	1.472	0	**C6**	-0.717	-0.098	0	**C6**	0	-0.736	0
C7	0.676	2.696	0	**C7**	1.548	-1.004	0	**C7**	0	1.46	-1.207
C8	-0.695	-2.23	0	**C8**	-1.548	1.004	0	**C8**	0	-1.46	-1.207
C9	-0.676	2.696	0	**C9**	1.253	1.465	0	**C9**	0	1.46	1.207
C10	0.695	-2.23	0	**C10**	-1.253	-1.465	0	**C10**	0	-1.46	1.207
C11	2.804	1.505	0	**C11**	1.023	-2.337	0	**C11**	0	0.77	-2.518
C12	-2.881	-1.054	0	**C12**	-1.023	2.337	0	**C12**	0	-0.77	-2.518
C13	2.881	-1.054	0	**C13**	-0.315	-2.559	0	**C13**	0	0.77	2.518
C14	-2.804	1.505	0	**C14**	0.315	2.559	0	**C14**	0	-0.77	2.518
C15	3.621	0.299	0	**C15**	3.021	-0.825	0	**C15**	0	2.858	-1.199
C16	-3.621	0.299	0	**C16**	-3.021	0.825	0	**C16**	0	-2.858	-1.199
H17	1.225	3.634	0	**C17**	2.603	1.702	0	**C17**	0	2.858	1.199
H18	-1.263	-3.155	0	**C18**	-2.603	-1.702	0	**C18**	0	-2.858	1.199
H19	-1.225	3.634	0	**C19**	3.573	0.623	0	**C19**	0	3.561	0
H20	1.263	-3.155	0	**C20**	-3.573	-0.623	0	**C20**	0	-3.561	0
H21	-3.338	2.451	0	**H21**	1.736	-3.155	0	**H21**	0	3.37	-2.157
H22	3.338	2.451	0	**H22**	-1.736	3.155	0	**H22**	0	-3.37	-2.157
O23	3.509	-2.09	0	**H23**	-0.711	-3.57	0	**H23**	0	3.37	2.156
O24	-3.509	-2.09	0	**H24**	0.711	3.57	0	**H24**	0	-3.37	2.156
O25	4.838	0.323	0	**H25**	2.994	2.716	0	**H25**	0	4.647	0
O26	-4.838	0.323	0	**H26**	-2.994	-2.716	0	**H26**	0	-4.647	0
CAP				**CAT**				**PST**			
	X	Y	Z		X	Y	Z		X	Y	Z
O1	-3.843	1.472	0	**O1**	3.565	1.372	0	**O1**	-3.49	-2.373	-0.001
O2	3.843	1.472	0	**O2**	3.565	-1.372	0	**O2**	3.49	-2.373	-0.004
O3	-3.843	-1.472	0	**O3**	-3.565	1.372	0	**O3**	-3.49	2.373	-0.002
O4	3.843	-1.472	0	**O4**	-3.565	-1.372	0	**O4**	3.49	2.373	-0.003
C5	-0.69	0	0	**C5**	0	0.669	0	**O5**	-4.875	0	0.005
C6	0.69	0	0	**C6**	0	-0.669	0	**O6**	4.875	0	0.007
C7	-1.413	1.205	0	**C7**	1.187	1.476	0	**C7**	-0.716	0	0
C8	1.413	1.205	0	**C8**	-1.187	1.476	0	**C8**	0.716	0	0
C9	-1.413	-1.205	0	**C9**	1.187	-1.476	0	**C9**	-1.402	-1.251	0
C10	1.413	-1.205	0	**C10**	-1.187	-1.476	0	**C10**	1.402	-1.251	-0.001
C11	-2.847	0.798	0	**C11**	2.5	-0.799	0	**C11**	-1.402	1.251	-0.001

C12	2.847	0.798	0	**C12**	-2.5	-0.799	0	**C12**	1.402	1.251	0
C13	-2.847	-0.798	0	**C13**	-2.5	0.799	0	**C13**	-0.699	-2.442	-0.001
C14	2.847	-0.798	0	**C14**	2.5	0.799	0	**C14**	0.699	-2.442	-0.001
C15	-0.713	2.402	0	**C15**	0.735	2.774	0	**C15**	-0.699	2.442	-0.001
C16	0.713	2.402	0	**C16**	-0.735	2.774	0	**C16**	0.699	2.442	-0.001
C17	-0.713	-2.402	0	**C17**	0.735	-2.774	0	**C17**	-2.886	-1.324	0
C18	0.713	-2.402	0	**C18**	-0.735	-2.774	0	**C18**	2.886	-1.324	-0.001
H19	-1.245	3.349	0	**H19**	1.348	3.668	0	**C19**	-2.886	1.324	-0.001
H20	1.245	3.349	0	**H20**	-1.348	3.668	0	**C20**	2.886	1.324	0
H21	-1.245	-3.349	0	**H21**	1.348	-3.668	0	**C21**	-3.673	0	0.002
H22	1.245	-3.349	0	**H22**	-1.348	-3.668	0	**C22**	3.673	0	0.003
								H23	-1.26	-3.371	-0.001
								H24	1.26	-3.371	-0.001
								H25	-1.26	3.371	-0.001
								H26	1.26	3.371	-0.001
BST-CN				**BST-NH_2**				**CAT-NH_2**			
	X	**Y**	**Z**		**X**	**Y**	**Z**		**X**	**Y**	**Z**
O1	3.584	-2.173	0.001	**O1**	-4.026	1.2	0	**O1**	1.395	-3.544	-0.004
O2	-3.584	2.173	0.001	**O2**	4.026	-1.2	0	**O2**	-1.395	-3.544	-0.004
O3	2.006	-4.413	0.001	**O3**	-4.656	-1.424	0	**O3**	1.395	3.544	0.004
O4	-2.006	4.413	0.001	**O4**	4.656	1.424	0	**O4**	-1.395	3.544	0.004
C5	0.33	-0.645	-0.001	**C5**	-0.707	-0.189	0	**C5**	0.67	0	0
C6	-0.33	0.645	-0.001	**C6**	0.707	0.189	0	**C6**	-0.67	0	0
C7	1.712	-0.726	0	**C7**	-1.681	0.788	0	**C7**	1.455	-1.179	-0.024
C8	-1.712	0.726	-0.001	**C8**	1.681	-0.788	0	**C8**	1.455	1.179	0.024
C9	-0.495	-1.861	0	**C9**	-1.059	-1.624	0	**C9**	-1.455	-1.179	-0.024
C10	0.495	1.861	0	**C10**	1.059	1.624	0	**C10**	-1.455	1.18	0.024
C11	2.527	0.463	0	**C11**	-1.321	2.204	0	**C11**	-0.8	-2.476	-0.011
C12	-2.527	-0.463	0	**C12**	1.321	-2.204	0	**C12**	-0.8	2.476	0.011
C13	1.938	1.706	0	**C13**	0.017	2.583	0	**C13**	0.8	2.476	0.011
C14	-1.938	-1.706	0	**C14**	-0.017	-2.583	0	**C14**	0.8	-2.476	-0.011
C15	2.381	-2.056	0	**C15**	-3.117	0.389	0	**C15**	2.778	-0.743	0.002
C16	-2.381	2.056	-0.001	**C16**	3.117	-0.389	0	**C16**	2.778	0.742	-0.002
C17	0.052	-3.113	0	**C17**	-2.382	-2.028	0	**C17**	-2.778	-0.743	0.002
C18	-0.052	3.113	0	**C18**	2.382	2.028	0	**C18**	-2.778	0.743	-0.002
C19	1.491	-3.314	-0.001	**C19**	-3.471	-1.109	0	**N19**	-3.896	1.506	0.017
C20	-1.491	3.314	-0.001	**C20**	3.471	1.109	0	**H20**	-3.75	2.503	-0.069
H21	-0.571	-4.003	0	**H21**	-2.641	-3.081	0	**H21**	-4.75	1.149	-0.383
H22	0.571	4.003	0	**H22**	2.641	3.081	0	**N22**	-3.896	-1.506	-0.017
C23	2.74	2.885	0	**N23**	2.267	-3.152	0	**H23**	-4.75	-1.149	0.383
N24	3.351	3.873	0.001	**H24**	3.243	-2.893	0	**H24**	-3.749	-2.503	0.069
C25	3.958	0.413	0	**N25**	-0.263	-3.986	0	**N25**	3.896	1.506	0.017
N26	5.113	0.535	0.001	**H26**	-0.78	-4.286	-0.821	**H26**	4.75	1.149	-0.382

C27	-3.958	-0.413	0	**N27**	0.263	3.986	0	**H27**	3.749	2.503	-0.069
N28	-5.113	-0.535	0	**H28**	0.781	4.286	0.821	**N28**	3.896	-1.506	-0.017
C29	-2.74	-2.885	0	**N29**	-2.267	3.152	0	**H29**	3.749	-2.504	0.069
N30	-3.351	-3.873	0	**H30**	1.932	-4.107	0	**H30**	4.75	-1.149	0.383
				H31	-0.781	-4.285	0.821				
				H32	-3.243	2.893	0				
				H33	0.781	4.286	-0.821				
				H34	-1.932	4.107	0				

CAT-CN			
	X	**Y**	**Z**
O1	-1.377	-3.564	0
O2	1.377	-3.564	0
O3	-1.377	3.564	0
O4	1.377	3.564	0
C5	-0.673	0	0
C6	0.673	0	0
C7	-1.47	-1.188	0
C8	-1.47	1.188	0
C9	1.47	-1.188	0
C10	1.47	1.188	0
C11	0.796	-2.508	0
C12	0.796	2.508	-0.001
C13	-0.796	2.508	-0.001
C14	-0.796	-2.508	0
C15	-2.775	-0.748	0
C16	-2.775	0.748	0
C17	2.775	-0.748	0
C18	2.775	0.748	0
C19	3.957	1.524	0
C20	3.957	-1.524	0
C21	-3.957	1.524	0
C22	-3.957	-1.524	0
N23	4.948	2.131	0
N24	4.948	-2.131	0
N25	-4.948	2.131	0
N26	-4.948	-2.131	0

Reference

[1] P. F. Wang, H. Xin, T. T. Zuo, Q. Li, X. Yang, Y. X. Yin, X. Gao, X. Yu and Y. G. Guo, An Abnormal 3.7 Volt O3-Type Sodium-Ion Battery Cathode, *Angew. Chem. Int. Ed.*, 2018, **57**,8178–8183, DOI: 10.1002/anie.201804130.

[2] E. de la Llave, E. Talaie, E. Levi, P. K. Nayak, M. Dixit, P. T. Rao, P. Hartmann, F. Chesneau, D. T. Major, M. Greenstein, D. Aurbach and L. F. Nazar, Improving Energy Density and Structural Stability of Manganese Oxide Cathodes for Na-Ion Batteries by Structural Lithium Substitution, *Chem. Mater.*, 2016, **28**, 9064–9076, DOI: 10.1021/acs.chemmater.6b04078.

[3] Y. Liu, X. Fang, A. Zhang, C. Shen, Q. Liu, H. A. Enaya and C. Zhou, Layered P2-$Na_{2/3}[Ni_{1/3}Mn_{2/3}]O_2$ as High-voltage Cathode for Sodium-ion Batteries: The Capacity Decay Mechanism and Al_2O_3 Surface Modification, *Nano Energy*, 2016, **27**, 27–34, DOI: 10.1016/j.nanoen.2016.06.026.

[4] T. Song, W. Yao, P. Kiadkhunthod, Y. Zheng, N. Wu, X. Zhou, S. Tunmee, S. Sattayaporn and Y. Tang, A Low-Cost and Environmentally Friendly Mixed Polyanionic Cathode for Sodium-Ion Storage, *Angew.Chem.*, 2020, **132**,750–755, DOI: 10.1002/ange.201912272.

[5] N. Yabuuchi, M. Kajiyama, J. Iwatate, H. Nishikawa, S. Hitomi, R. Okuyama, R. Usui, Y. Yamada and S. Komaba, P2-type $Na_x[Fe_{1/2}Mn_{1/2}]O_2$ Made from Earth-abundant Elements for Rechargeable Na Batteries, *Nat Mater*, 2012, **11**, 512–517, DOI: 10.1038/nmat3309.

[6] W. Li, C. Han, W. Wang, Q. Xia, S. Chou, Q. Gu, B. Johannessen, H. Liu and S. Dou, Stress Distortion Restraint to Boost the Sodium Ion Storage Performance of a Novel Binary Hexacyanoferrate, *Adv. Energy Mater.*, 2020, **10**, 1903006, DOI: 10.1002/aenm.201903006.

[7] P. F. Wang, Y. You, Y. X. Yin, Y. S. Wang, L. J. Wan, L. Gu and Y. G. Guo, Suppressing the P2-O2 Phase Transition of $Na_{0.67}Mn_{0.67}Ni_{0.33}O_2$ by Magnesium Substitution for Improved Sodium-Ion Batteries, *Angew. Chem. Int. Ed.*, 2016, **55**,7445–7449, DOI: 10.1002/ange.201602202.

[8] P. Hu, C. Cai, X. Li, Z. Wei, M. Wang, C. Chen, T. Zhu, L. Mai and L. Zhou, V Doping in NASICON-Structured $Na_3MnTi(PO_4)_3$ Enables High-Energy and Stable Sodium Storage, *Adv. Funct. Mater.*, 2023, **34**, 2302045, DOI: 10.1002/adfm.202302045.

[9] C. Fang, Y. Huang, L. Yuan, Y. Liu, W. Chen, Y. Huang, K. Chen, J. Han, Q. Liu and Y. Huang, A Metal-Organic Compound as Cathode Material with Super high Capacity Achieved by Reversible Cationic and Anionic Redox Chemistry for High-Energy Sodium-Ion Batteries, *Angew. Chem. Int. Ed.*, 2017, **56**, 6793–

6797, DOI: 10.1002/ange.201701213.

[10] H. Banda, D. Damien, K. Nagarajan, M. Hariharan and M. M. Shaijumon, A Polyimide Based All-organic Sodium Ion Battery, *J. Mater. Chem. A*, 2015, **3**, 10453, DOI: 10.1039/C5TA02043C.

[11] Q. Zhao, W. Zhao, C. Zhang, Y. Wu, Q. Yuan, A. K. Whittaker and X. S. Zhao, Sodium-Ion Storage Mechanism in Triquinoxalinylene and a Strategy for Improving Electrode Stability, *Energy Fuels*, 2020, **34**, 5099–5105, DOI: 10.1021/acs.energyfuels.0c00798.

[12] C. Huangfu, Z. Liu, X. Lu, Q. Liu, T. Wei, Z. Fan, Strong Oxidation Induced Quinone-rich Dopamine Polymerization onto Porous Carbons as Ultrahigh-capacity Organic Cathode for Sodium-ion Batteries, *Energy Storage Materials*, 2021, **43**, 120–129, DOI: 10.1016/j.ensm.2021.08.043.

[13] Y. Chen, Q. Zhu, K. Fan, Y. Gu, M. Sun, Z. Li, C. Zhang, Y. Wu, Q. Wang, S. Xu, J. Ma, C. Wang and W. Hu, Successive Storage of Cations and Anions by Ligands of π-d-Conjugated Coordination Polymers Enabling Robust Sodium-Ion Batteries, *Angew. Chem. Int. Ed.*, 2021, **60**, 18769–18776, DOI: 10.1002/anie.202106055.

[14] X. Zhao, W. Qiu, C. Ma, Y. Zhao, K. Wang, W. Zhang, L. Kang and J. Liu, Superposed Redox Chemistry of Fused Carbon Rings in Cyclooctatetraene-Based Organic Molecules for High-Voltage and High-Capacity Cathodes, *ACS Appl. Mater. Interfaces*, 2018, **10**, 2496–2503, DOI: 10.1021/acsami.7b15495.

[15] K. C. Kim, T. Liu, K. H. Jung, S. W. Lee and S. S. Jang, Unveiled Correlations between Electron Affinity and Solvation in Redox Potential of Quinone-based Sodium-ion Batteries, *Energy Storage Materials*, 2019, **19**, 242–250, DOI: 10.1016/j.ensm.2019.01.017.

[16] G. S. Jeong, K. H. Jung, S. Choi and K. C. Kim, Electrochemical Characteristics of Cyanoquinones as Organic Cathodes for High-Potential Sodium-Ion Batteries, *ACS Sustainable Chem. Eng.*, 2020, **8**, 11328–11336, DOI: 10.1021/acssuschemeng.0c03332.

[17] K. C. Kim, T. Liu, S. W. Lee and S. S. Jang, First-Principles Density Functional Theory Modeling of Li Binding: Thermodynamics and Redox Properties of Quinone Derivatives for Lithium-Ion Batteries, *J. Am. Chem. Soc.*, 2016, **138**, 2374-2382, DOI: 10.1021/jacs.5b13279.

[18] T. Yokoji, Y. Kameyama, N. Maruyama and H. Matsubara, High-Capacity Organic Cathode Active Materials of 2,2′-Bis-P-Benzoquinone Derivatives for Rechargeable Batteries, *J. Mater. Chem. A*, 2016, **4**, 5457-5466, DOI: 10.1039/C5TA10713J.

[19] H. Roth, N. Romero and D. Nicewicz, Experimental and Calculated Electrochemical Potentials of Common Organic Molecules for Applications to Single-Electron Redox Chemistry, *Synlett*, 2015, **27**, 714-723, DOI:

10.1055/s-0035-1561297.

[20] R. B. Araujo, A. Banerjee, P. Panigrahi, L. Yang, M. Strømme, M. Sjödin, C. M. Araujo and R. Ahuja, Designing Strategies to Tune Reduction Potential of Organic Molecules for Sustainable High Capacity Battery Application, *J. Mater. Chem. A*, 2017, **5**, 4430-4454, DOI: 10.1039/C6TA09760J.

[21] W. Wan, H. Lee, X. Yu, C. Wang, K.-W. Nam, X.-Q. Yang and H. Zhou, Tuning The Electrochemical Performances of Anthraquinone Organic Cathode Materials for Li-Ion Batteries through The Sulfonic Ssodium Functional Group, *RSC Adv.*, 2014, **4**, 19878-19882, DOI: 10.1039/C4RA01166J.

[22] T. Ma, Q. Zhao, J. Wang, Z. Pan and J. Chen, A Sulfur Heterocyclic Quinone Cathode and A Multifunctional Binder for A High-Performance Rechargeable Lithium-Ion Battery, *Angew. Chem. Int. Ed.*, 2016, **55**, 6428-6432, DOI: 10.1002/anie.201601119.

[23] Y. Liang, P. Zhang, S. Yang, Z. Tao and J. Chen, Fused Heteroaromatic Organic Compounds for High-Power Electrodes of Rechargeable Lithium Batteries, *Adv. Energy Mater.*, 2013, **3**, 600-605, DOI: 10.1002/aenm.201200947.

[24] B. Tian, Z. Ding, G. H. Ning, W. Tang, C. Peng, B. Liu, J. Su, C. Su and K. P. Loh, Amino Group Enhanced Phenazine Derivatives as Electrode Materials for Lithium Storage, *Chem. Commun.*, 2017, **53**, 2914-2917, DOI: 10.1039/C6CC09084B.

[25] Y. Lu, Q. Zhang, L. Li, Z. Niu and J. Chen, Design Strategies Toward Enhancing The Performance of Organic Electrode Materials in Metal-Ion Batteries, *Chem*, 2018, **4**, 2786-2813, DOI: 10.1016/j.chempr.2018.09.005.

[26] Y. Morita, S. Nishida, T. Murata, M. Moriguchi, A. Ueda, M. Satoh, K. Arifuku, K. Sato and T. Takui, Organic Tailored Batteries Materials Using Stable Open-Shell Molecules with Degenerate Frontier Orbitals, *Nat. Mater.*, 2011, **10**, 947-951, DOI: 10.1038/nmat3142.

[27] K. C. Kim, T. Liu, K. H. Jung, S. W. Lee and S. S. Jang, Unveiled correlations between electron affinity and solvation in redox potential of quinone-based sodium-ion batteries, *Energy Storage Mater.*, 2019, **19**, 242-250, DOI: 10.1016/j.ensm.2019.01.017.

[28] R. B. Araujo, A. Banerjee, P. Panigrahi, L. Yang, M. Strømme, M. Sjödin, C. M. Araujo and R. Ahuja, Designing strategies to tune reduction potential of organic molecules for sustainable high capacity battery application, *J. Mater. Chem. A*, 2017, **5**, 4430-4454, DOI: 10.1039/C6TA09760J.